Lung-targeted Macrophage Biomimetic Nanocarriers Based on Platycodon Grandiflorum Polysaccharides for Calming Cytokine Storm in Pneumonia

Yi Li
Yantai University
Chunjing Guo
Ocean University of China
Qiang Chen
Yantai University
Yanguo Su
Yantai University
Huimin Guo
Yantai University
Daquan Chen (cdq1981@126.com)
Yantai University https://orcid.org/0000-0002-6796-0204

Research Article

Keywords: Acute lung injury, Platycodon grandiflorum polysaccharides, Biomimetic, Medicinal guide theory, Cytokine storms

Posted Date: November 15th, 2021

DOI: https://doi.org/10.21203/rs.3.rs-1053318/v1

Abstract

Background

Pneumonia is a life-threatening respiratory disease without effective treatment due to uncontrolled inflammation of the lung tissue. Suppression of cytokine storms may be one of the keys to saving the lives of patients with severe pneumonia. Given the fragile delivery efficiency of drugs in vivo, novel delivery platforms to address these issues are necessary.

Results

Here, we developed a biomimetic nanocarrier (MNPs) with macrophage membranes coated ROS-responsive Platycodon grandiflorum polysaccharides nanoparticles (PNPs) for targeted delivery of curcumin (MNPs@Cur) to inflamed lungs and treat inflammation by calming cytokine storms. In the study, we could clearly find that MNPs@Cur significantly attenuated inflammation and cytokine storm syndrome in acute lung injury (ALI) mice by neutralizing multiple proinfammatory cytokines. Interestingly, we found that the PNPs also had potent pulmonary targeting compared to other polysaccharide carriers, which probably means that PNPs have inherited the natural targeting ability in the medicinal guide theory of Traditional Chinese Medicine (TCM).

Conclusion

The results demonstrated that the developed drug delivery system may serve as an effective and safe nanoplatform for the treatment of pneumonia, as well as provide experimental scientific basis for the medicinal guide theory of TCM and its clinical application.

Background

Inflammation is a defense mechanism that protects body from damage caused by infections and tissue injury. However, uncontrolled hyperinflammation can also induce an overwhelming local/systemic inflammatory response leading to life-threatening diseases such as pneumonia, acute lung injury (ALI), which can rapidly cause acute respiratory distress syndrome (ARDS)[1]. For example, the novel coronavirus disease 2019 (COVID-19), which is spreading worldwide, has infected more than 170 million people and killed more than 3.5 million of people in worldwide so far. Based on current clinical studies, sudden exacerbations in patients with their infections have been found to be closely associated with cytokine storm, which marks an uncontrolled and dysfunctional immune response that will likely lead to serious consequences and even death[2].

More and more evidences indicate that suppression of cytokine storm may be o one key to save the life of patients with severe pneumonia[3, 4]. Currently, glucocorticoids are used in the treatment of heavy and

critical cases in the existing protocols to exert immunosuppressive effects and to control cytokine storm[5, 6]. Although promising, frequent long-term use or high doses of glucocorticoids may lead to the risk of serious complications and sequelae, such as osteonecrosis and hyperglycemia[7, 8]. Meanwhile, advanced techniques have been developed in lung-protected ventilation as well as nebulization, but to increase the efficiency of inhalation, part of the machine parameters need to be adjusted or sedative drugs need to be given, which may further prolong the duration of mechanical ventilation for the patient, which would increase the discomfort and the cost for the patient[9, 10]. In addition, there is a demand for further development of microenvironment-responsive targeted drug delivery systems to modulate the local inflammatory immune response to improve the inflammatory microenvironment (IME) at the lesions considering the unique characteristics of the IME[11, 12], including low pH and overproduction of reactive oxygen species (ROS), thus improving the therapeutic efficacy as well as reducing the toxic side effects.

In light of the Traditional Chinese Medicine (TCM) played a significant role in this control and treatment of this epidemic, for example, Qingfei Paidu Decoction has become an important tool in the treatment of COVID-19[13, 14]. It was found that in the face of complex pathogenesis of cytokine storm, active ingredients of TCM with multiple targets can be more advantageous than chemical drugs with clear targets through holistic modulation[15]. Curcumin (Cur), a natural plant extract, has been shown to inhibit viral infections, reduce the severity of lung injury and inhibit subsequent fibrosis by calming down cytokine storm, thereby increasing survival rates and improving symptoms in mice with pneumonia[16]. The medicinal guide theory plays important role in the concept of, mainly guiding the drugs in the prescription, which can lead other drugs to the lesion and change the direction or site of action of other herbs, or make their action focused or concentrated in a specific direction and site. For instance, Platycodon grandiflorum leads medicine to the lung and borneol leads medicine to the brain[17, 18]. The medicinal guide theory of TCM is similar to the targeted action of modern preparations[19]. The difference is that the targeting effect of modern pharmaceuticals is mostly artificially added to the targeting nature of a certain carrier, while TCM medicinal guide theory has natural active targeting characteristics. We previously constructed a nano-platform to investigate targeted therapy for liver cancer using liver-targeted Angelica polysaccharide (AP) as the main component[20]. Platycodon grandiflorum polysaccharide (PGP), as the active ingredient of Platycodon grandiflorum, has been studied mostly for its pharmacological effects such as antitumor, anti-inflammatory and antioxidant[21, 22], while the study as a drug delivery vehicle is currently a complete blank. Inspired by the hepatic targeting ability of AP and the unique IME, ROS-responsive strategies based on PGP can be developed for drug delivery in lung diseases.

Cellular delivery systems are received mounting interest for their excellent biocompatibility and exceptional drug delivery behavior[23, 24]. Macrophages as one of inherent cells in the body, which can act as drug delivery systems are equipped with several advantages compared with other synthetic delivery systems[25]. For instance, as a role of immune cells, macrophages have an intrinsic affinity for sites of inflammation, and chemokines on the surface of macrophage membranes (MM) such as chemokine receptors CCR2, CCR6 and CXCR1 can trigger macrophages to adhere to inflammatory or tumor sites[26, 27]. Simon et al[28]. recently revealed that MM-encapsulated drug delivery methods may

be more suitable than macrophage internalized with nanoparticles for the treatment of inflammatory diseases, demonstrating the broad promise of cell membrane-coated nanoparticles. Wang et al[29]. utilized MM-encapsulated nanoparticles loaded with rapamycin for targeted treatment of atherosclerosis and exhibited outstanding efficacy. Zhang et al[30]. reported a multi-antigen nano-toxin vaccine based on MM-encapsulated nanoparticles to combat inflammatory lung infections. There is a growing amount of evidence that MM-coated drug delivery systems may be a powerful platform for targeted inflammatory therapies.

In this study, given the important role of macrophages in the inflammatory process, we attempted to structure dual targeting biomimetic drug delivery system (MNPs) with MM coating for targeted therapy of pneumonia. The core is a ROS-responsive nanoparticle loaded with Cur (PNPs@Cur) constructed on the basis of PGP, which achieves precise drug release at the site of inflammation (Scheme 1). Interestingly, we discovered that PGP nanoparticles (PNPs) were also efficiently aggregated in the lungs of model mice compared to the control group. In mice models of ALI, we systematically evaluated the targeting efficiency and therapeutic efficacy of PNPs@Cur and MM coated PNPs@Cur (MNPs@Cur), significantly reducing inflammation and cytokine storm syndrome and alleviating symptoms in mice with ALI compared to the free drug group. We hypothesized that MNPs@Cur, which possess the dual targeting of TCM channel ushering and macrophage intrinsic chemotaxis, could more effectively accumulate in the damaged lung and thus effectively inhibit the progression of lung disease.

Results And Discussion

Synthesis and characterization of PNPs and MNPs

Firstly, we obtained the amphiphilic carrier material Oxi-PGP by structural modification of PGP, followed by self-assembly to obtain nanoparticles (PNPs) with ROS responsiveness. The synthesis process of the carrier materials is shown in Fig. 1a. The successful construction of Oxi-PGP was verified by ^{1}H NMR (Fig. 1b), the peaks appearing at 3.0-4.0 ppm and 7.0-8.2 ppm belonged to PGP as well as ROS-responsive groups, respectively. The marked decrease in the absorption peak of hydroxyl group at 3300 cm^{-1} and the appearance of carbonyl and phenyl characteristic peaks at 1748 cm^{-1} and 1650-1500 cm^{-1} in Fourier transform infrared spectroscopy (FT-IR) further confirmed the successful preparation of the carrier material (Fig. 1c)). Subsequently, the drug encapsulation efficiency (EE) and drug loading efficiency (DLC) of PNPs@Cur were 76.6% and 11.3%, respectively, obtained by HPLC, indicating the successful drug encapsulation. Dynamic light scattering (DLS) analysis showed that the hydrodynamic diameter of PNPs was about 91.1 nm, the PDI was 0.139 (Fig. 2a). Transmission electron microscopy (TEM) indicated that these PNPs particles had a spherical structure with a particle size of about 80 nm (Fig. 2d).

The ROS-responsive drug delivery system constructed in this study, as its hydrophobic core phenylborate polymer could be degraded under H_2O_2 conditions, disrupted the nanoparticle structure allowing precise drug release in the inflammatory microenvironment. To investigate the ROS responsiveness of PNPs, we

selected phosphate-buffered saline (PBS) containing different concentrations of H_2O_2 to measure the degree of hydrolysis of nanoparticles at predetermined time points, namely the change in transmittance at 500 nm. The H_2O_2 concentrations used in this study were based on previous simulated in vitro inflammatory lesion tissue H_2O_2 levels[31]. As illustrated in Fig. 2c, the degree of hydrolysis of PNPs gradually increased with increasing H_2O_2 concentration, and the particle solution was almost completely transparent within 3 h at 1.00 mM concentration. In contrast, the particles in PBS exhibited only a moderate decrease in absorbance within 6 h due to the partial precipitation of PNPs. With the gradual structural disruption of the nanoparticles, the release of the drug should be increased. This speculation was subsequently confirmed by our in vitro cumulative release profiles at different H_2O_2 concentrations (Fig. 2f). At a concentration of 1.00 mM H_2O_2, PNPs@Cur exhibited a cumulative drug release rate of up to 76%, however, only about 20% of the drug was released in the absence of peroxide treatment. Collectively we have successfully constructed ROS-responsive drug delivery systems.

In order to acquire MNPs, the macrophage membranes were first oscillatory fused with PNPs in ultrasound and then passed through 400 and 200 nm polycarbonate porous membranes by extrusion, respectively. Compared with the uncoated PNPs, DLS (Fig. 2b) indicated that the MNPs hydrodynamic diameter increased from 91.1 nm to 125.3 nm with a more negative zeta potential, which was closer to the zeta potential of the macrophage surface (Figs. 2g, h). Within the TEM images MNPs exhibited a spherical core-shell structure (Fig. 2e), each nanoparticle was encapsulated by a single layer of cell membrane, and the coating thickness of the nanoparticles was about 9 nm, consistent with the thickness of the cell membrane, suggesting a successful wrap of the cell membrane. Furthermore, the presence of the key membrane antigen CCR2 (receptor for monocyte chemoattractant protein-1 (MCP-1)), which tends immune cells to the site of inflammation, was detected by Western blot on the surfaces of macrophages, macrophage membranes, and MNPs. In contrast, β-Actin was largely absent compared to macrophages, demonstrating the higher purity of macrophage membrane extraction. Moreover, no protein signal was detected from PNPs, further indicating that macrophage membranes were successfully coated and maintained on the surface of MNPs (Figs. 3b-d). PNPs@Cur and MNPs@Cur both exhibited relatively stable sizes in PBS containing 10% fetal bovine serum (FBS) after long-term storage at room temperature, indicating satisfactory stability (Fig. 3a). We also examined the in vitro release of MNPs@Cur and the release rate of MNPs@Cur was quite similar to that of PNPs@Cur under the same conditions (Fig. 2i), indicating that the macrophage membrane coating had no significant effect on the responsiveness of PNPs to the inflammatory microenvironment.

In vitro binding to the site of inflammation

Whether the drug delivery system could be taken up by target cells is a prerequisite for maximizing drug efficacy and reducing side effects on other tissues and organs. Therefore, it is an essential indicator to avoid phagocytosis by macrophages of the reticuloendothelial system to verify the drug delivery system. There is increasing evidence that MM-encapsulated nanoparticles can prevent the phagocytosis of macrophages[32, 33]. As the model drug Cur itself is fluorescent, the uptake efficiency of MNPs@Cur,

PNPs@Cur was evaluated in RAW264.7 cells, respectively, with the free drug as a control group. We could find a time-dependent uptake in each group (Fig. 4a), but intense green fluorescence could be observed in macrophages incubated with free Cur for 4 h, apparently indicating that the free drug was taken up by macrophages. In contrast, little fluorescence was observed in macrophages cultured with MNPs@Cur, implying that the drug delivery system wrapped by the macrophage membrane may be an effective strategy to evade macrophage clearance. Interestingly, we found that less fluorescence was also present in the PNPs@Cur incubation group. To further investigate the uptake mechanism, CNPs@Cur was used for comparison, and PNPs@Cur could also be effective for cellular escape (Fig. 5a), the result demonstrated that PNPs@Cur might also has better drug delivery properties.

Subsequently, we validated whether MNPs@Cur can effectively target damaged inflammatory cells. The conversion of RAW264.7 cells into activated macrophages was induced by LPS thus to simulate the establishment of a cellular inflammation model[34, 35]. It was evident that intense fluorescence could be observed in MNPs@Cur incubation (Fig. 4b), indicating a significant uptake by inflammatory macrophages, implying no discrimination against macrophage-membrane coated nanoparticles. To further verify the targeting of MNPs@Cur, the targeting effect was observed in activated HUVECs (Fig. 4c), where endothelial cells also play a major role in the inflammation initiation process. The targeting ability of MNPs@Cur could be significantly observed in both groups of inflammatory cells, indicating the chemotaxis of CCR-2 on the surface of macrophages to the site of inflammation, directing the binding to inflammatory cells. Meanwhile, it was also found that PNPs@Cur had relatively strong inflammatory targeting ability, and further compared with CNPs@Cur (Fig. 5b). Considering the previous cell escape ability, we suggested that PNPs have better inflammatory cell targeting ability compared with CNPs. The intracellular fluorescence intensity of CNPs@Cur may be a result of the positive charge on the surface of their particles, allowing them to be readily taken up by various cells. These results suggested that PNPs also showed affinity for major components of inflammation-related cells in vitro, which may be attributed to the receptor/protein binding mechanism between the monosaccharide portion of PGP therein and inflammatory cells. Certainly, this speculation still needs further deeper excavation to provide stronger scientific support for the guide theory of Platycodon grandiflorum.

To further investigate the intracellular release behavior of the drug, NR fluorescent probes which barely fluoresce in polar solutions but have intense red fluorescence in the lipid environment were selected to observe the release state in inflammatory cells. MNPs@NR were co-incubated with activated macrophages. As shown in the Fig. 4d, the red fluorescence of NR being excited in inflammatory cells is increasing in a time-dependent manner. Generally, the wrapping of macrophage membranes allowed MNPs to effectively avoid uptake by macrophages, thereby further enhanced targeting to inflammatory cells, and implied that MNPs@Cur could release drugs precisely at the site of inflammation, avoiding side effects at other sites. More astonishingly, PNPs also possess this kind of superiority compared to CNPs, only that their intrinsic mechanisms need to be studied more diligently. The ROS-responsive PNPs coated with macrophage membranes constructed in this study with dual targeting may provide a potential platform for improved therapeutic targeting of inflammation.

In vitro assessment of safety and anti-inflammatory effects

Then, the safety of PNPs as well as MNPs was verified by systematically assessing their biocompatibility in vitro. HUVECs and RAW264.7 cells were incubated with media containing different concentrations of PNPs and MNPs for 48 hours to assess their cytotoxicity. These results showed (Figs. 6a, b) favorable cytocompatibility in all experimental groups compared to the control group.

The other important indicator of biomaterials, blood compatibility, further confirmed the safety of the carrier material. Therefore, PNPs as well as MNPs were evaluated in vitro to evaluate whether hemolysis could be avoided. Hemolysis of PNPs and MNPs was examined by direct contact method. As shown in Fig. 6c, PNPs and MNPs were not significantly different from the negative control, with hemolysis rates even lower than 0.5% (Fig. 6d). Considering the above, the results of cytotoxicity as well as hemocompatibility confirmed the superior biocompatibility of the carriers.

The cytokines and pro-inflammatory mediators released by macrophages play an important role in the pathogenesis of ALI[36]. Cur is a natural phenolic compound with various pharmacological effects such as anti-inflammatory, antioxidant, anti-proliferative and anti-angiogenic. The appearance of cytokine storm is an important reason for the sudden exacerbation of the disease in many COVID-19 patients. Therefore, blocking cytokine storms is one of the key strategies to save patients' lives. It has been reported that IL-6 and TNF-α are key factors in triggering inflammatory storms[3, 4]. We investigated the ability of MNPs@Cur to block the cytokine storm at the cellular level (Figs. 6e, f), under the induction of LPS, a significant production of pro-inflammatory factors TNF-α and IL-6 by activated macrophages could be observed, however, their levels were decreased in all drug-treated groups, indicating the anti-inflammatory capacity of Cur. The downregulated levels of MNPs@Cur and PNPs@Cur were closer to the control group compared to the free drug, indicated a considerable accumulation and efficacy of the drug within the inflammatory cells, consistent with previous cellular uptake imaging results. Collectively, these results demonstrated the superior biocompatibility of PNPs and MNPs and further showed the excellent targeting ability of the constructed nanosystems on inflammatory cells to calm the cytokine storm.

Biodistribution in vivo

Given that MNPs exhibit significant ability to target inflammatory cells in vitro, we next investigated whether the lungs of inflamed mice could be specifically targeted in vivo. ALI mice were constructed and free DiR, CNPs@DiR, PNPs@DiR and MNPs@DiR (same dose of DiR) were injected intravenously into the mice in random groups, with healthy mice as controls. After 3 h of administration, the lung tissues collected from each group were imaged by IVIS, and it was observed (Fig. 7a) that MNPs@DiR showed the strongest fluorescence intensity in the lungs of inflamed mice compared with the fluorescence in the lungs of healthy mice or ALI mice from other dosing treatment groups, indicating that MNPs@DiR specifically targets the inflamed lungs of mice. Notably, the fluorescence intensity of PNPs@DiR was second only to that of MNPs@DiR (Fig. 7c). Consistent with previous cellular targeting results, the stronger fluorescence intensity of PNPs@DiR compared with DiR and CNPs@DiR implies that PNPs have the potential function of guiding drugs into the damaged lungs more than CNPs. It was consistent with

the theory that Platycodon grandiflorum guides drugs into the lung, implying that PGP may be one of the vital channel ushering components of Platycodon grandiflorum. Meanwhile, in the DiR-injected ALI mice, the fluorescent signal at 3 h was aggregated in the liver as well as the spleen. The weaker fluorescence intensity of DiR in PNPs@DiR, taken up by the liver and spleen, and the least fluorescence signal in MNPs@DiR-treated ALI mice was essentially present only in the liver, suggesting that after being coated by MM (Figs. 7b, d), MNPs are more likely to achieve immune escape and thus enhance the accumulation to inflamed lungs.

These results can be explained by the intrinsic affinity of macrophages for sites of inflammation. They can bind to activated/inflamed vessel walls through a range of receptor modes, including the chemokine receptor CCR2 and adhesion factors on the cell membrane surface. Furthermore, the temporary vasodilation and leakage of blood vessels induced by histamine at the time of injury allows injected nanoscale MNPs to passively target inflamed lung tissue through the vessels to the injured tissue. Regarding the pulmonary targeting ability of PNPs, we hypothesized that the monosaccharide component of PGP binds to receptors overexpressed on the surface of affected lung tissues and possesses the ability of PNPs to deliver drugs to the lung, and the specific targeting mechanism still needs further study. Conclusively, the ROS-responsive PNPs coated with macrophage membranes constructed in this study possessing dual targeting may provide a potential targeting delivery platform for improving the treatment of lung inflammation.

Improved treatment of acute pneumonia with MNPs@Cur

As previously mentioned, prevention or inhibition of cytokine storm may be one of the key strategies to save the lives of patients with severe pneumonia. Therefore, we investigated whether cytokine storms could be calmed by targeting MNPs@Cur to pneumonia sites. Fig. 8a shows the experimental protocol. To verify the efficacy of model drug-targeted delivery, mice were treated with LPS (10 mg/kg) to induce ALI. 5 h later, saline, free Cur (30 mg/kg), PNPs@Cur and MNPs@Cur (equivalent to 30 mg/kg of Cur) were injected intravenously and all mice were euthanized 19 h after injection for analysis. The lung tissue homogenate levels of TNF-α and IL-6 in the different treatment groups were analyzed separately using ELISA kits. Although Cur has been shown to reduce cytokine storm in previous studies, in our experimental mouse model of ALI, Cur had limited therapeutic effect and treatment with free curcumin modestly reduced cytokine levels. Encouragingly, treatment with MNPs@Cur resulted in a significant decrease in these inflammatory factors compared to the free drug group, demonstrating that targeted delivery of MNPs@Cur could effectively inhibit cytokine storm (Figs. 8b, c), which again confirms the superior inflammatory lung targeting ability of this combined dual-targeting bionic carrier.

In addition, we further measured the wet/dry weight ratio to observe the pulmonary edema. Pathological examination revealed edema in the lungs of COVID-19 patients, which may be due to excessive mucus secretion and infiltration of immune cells in the lungs. In the ALI mouse, we found excessive pulmonary edema, alveolar inflammatory cell exudation/infiltration and alveolar damage in lung tissue sections. By administration of different formulations and free drugs, we found that treatment with MNPs@Cur significantly reduced inflammatory cell infiltration in mice compared to the free drug group (Figs. 8g, h).

Meanwhile in the MNPs@Cur treatment group markedly improved the pulmonary edema status (Fig. 8d), and the wet/dry weight ratio of the lungs was more inclined to the normal group.

As a marker of neutrophil accumulation in inflammatory tissues, myeloperoxidase (MPO) levels can be assessed for the degree of migration and infiltration of neutrophils in inflammatory cells. As shown in the Fig. 8e, the MNPs@Cur treatment group remarkably repressed the migration and infiltration of inflammatory cells, which corresponded to the improvement of pulmonary edema. Given that oxidative stress is also part of the pathogenesis of ALI, malondialdehyde (MDA), a lipid peroxidation product, can reflect the level of ROS production from lipid oxidation. It was found that MDA was significantly elevated in the saline group Fig. 8f, indicating a redox imbalance and causing severe oxidative damage in AIL mice, and yet MNPs@Cur significantly inhibited the production of MDA compared with other groups, thus improving the microenvironment of oxidative stress in vivo. Above results showed that ROS were effectively eliminated in vivo by MPO and MDA, which are important defenses to mediate ROS in impaired lungs. The results of MPO and MDA, which are important defenses to neutralize impaired pulmonary ROS, indicated that the ROS were effectively cleared in vivo. Generally, the bionic drug delivery systems MNPs@Cur based on PGP can alleviate lung inflammation effectively, which means that MNPs can improve the pulmonary delivery of drugs and hence facilitate ALI treatment. Meanwhile, the results of H&E staining also showed no significant damage to major organs and immunotoxicity after treatment, which further validated the beneficial biocompatibility of our constructed drug delivery platform in vivo (Fig. 9).

Pneumonia is a serious respiratory disease that leads to high morbidity and mortality. Currently, few targeted therapeutic strategies are available, as specific delivery of drugs to the inflamed lungs remains challenging[37]. Although significant efforts have been made to develop effective pulmonary drug delivery systems, there is still a lack of nanodrug delivery systems that target the pathogenesis of lung inflammation. Combined with the presence of overexpressed ROS at the lesion site during pneumonia, this would allow pro-inflammatory factors to recruit macrophages to the lesion site as well as the guide theory of TCM. Therefore, we developed a ROS-responsive nanoparticle based on PGPs and coated MM on the surface of the nanoparticle to construct a bionic drug delivery system for lung diseases. Experiments were conducted sequentially at the cellular as well as animal levels to verify the excellent lung targeting ability and precise drug release. It provides inspiration for exploring other channel ushering components to construct natural drug targeting systems, and provides a strong experimental support for the modernization of Chinese medicine guide theory.

Conclusion

Collectively, inspired by the inherent affinity of macrophages for the site of inflammation and the guide theory of Platycodon grandiflorum. We have developed a PGP-based bionic drug delivery platform for the treatment of pneumonia. We found that MNPs can accumulate at sites of inflammation associated with pneumonia and facilitate delivery of anti-inflammatory drugs via intravenous administration (Fig. 10). It is emphasized by our results that targeted drug delivery for pneumonia significantly reduces cytokine

storm syndrome compared to free drug therapy. The prepared dual-targeted drug delivery platform perfectly combines modern bionic technology and TCM concepts and may provide a promising approach for the treatment of patients with COVID-19. Since the excellent biocompatibility and accessibility to preparation, it would provide a strong scientific basis for related TCM classical prescriptions and facilitates the search for natural targeted drug delivery systems, showing potential for further clinical translation.

Material And Methods

Materials

4-hydroxymethyl phenylboronic acid pinacol ester (4-PBAP) and N, N'-carbonyl diimidazole (CDI) were purchased from Aladdin (China). Platycodon grandiflorum polysaccharides were supplied by Shanghai Winherb Medical Technology Co., Ltd. 1,1-dioctadecyl-3,3,3,3-tetramethylindotricarbocyaine iodide (DiR) was obtained from Beijing Bioss Biotechnology Co. DAPI, Cell Total Protein Extraction kits, Bicinchoninic Acid Assay (BCA) protein assay kit and Membrane Protein Extraction kits were supplied by Beyotime Institute of Biotechnology (China). TNF-α and IL-6 ELISA kit were purchased from Beijing Solarbio Technology Co., Ltd. (China). Antibody CCR2 (anti-rabbit, #ABP53395) special for mouse were purchased from Abbkine (China), with a dilution ratio of 1:1000 for antibody. Antibodies β-Actin (#4967S) and HRP-conjugated anti-rabbit IgG (#7074) were purchased from Cell Signaling Technology (USA), with a dilution ratio of 1:1000 for both antibodies during experimental use. All other chemical reagents were supplied by Aladdin (China). All biological reagents, and other cell culture medium were used as received following our previous protocols.

Synthesis and characterization of copolymers.

The synthesis process was carried out according to the relevant literature[28, 38]. Briefly, the ROS reactive groups were first synthesized. The 4-hydroxymethylbenzeneboronic acid pinacol ester (4-PBAP, 5 mmol) and N, N'-carbonyl diimidazole (CDI, 10 mmol) were added to the reaction flask. After added 30 mL of anhydrous dichloromethane to fully dissolve the reaction and stirred at room temperature for 12 h, the unreacted raw material was washed with pure water (3×25 mL) followed by saturated NaCl (3×20 mL), discarded the aqueous layer and dried overnight under anhydrous Na_2SO_4. The ROS-responsive groups CDI-PBAP were obtained by reduced-pressure drying, and their chemical structures were characterized by NMR as well as IR spectroscopy.

To prepare modified Platycodon grandiflorum polysaccharides (Oxi-PGP), we performed structural modification of PGP by prepared CDI-PBAP, namely PGP (5 mmol) dissolved in formamide (4 mL), added DMAP (10 mmol) dissolved in anhydrous dimethyl sulfoxide (DMSO), and finally added CDI-PBAP (10 mmol), and stirred the mixture overnight at room temperature with a magnetic stirrer. Subsequently, the resulting solution was dialyzed in deionized water and centrifuged at 1500 rpm for 5 min to obtain the

supernatant, which was freeze-dried and prepared for use, and the successful synthesis of the modified product Oxi-PGP was verified by a series of characterizations.

Preparation and characterization of ROS responsive PNPs and PNPs@Cur

ROS-responsive nanoparticles were similarly prepared by dialysis. Oxi-PGP (10 mg) was weighed and dissolved in anhydrous DMSO (5 mL), and the resulting solution was dialyzed in deionized water (1000 mL) (MW: 8000-14000 Da) for 36 h, with water replacement at 4 h intervals. The final dialyzed solution was passed through the syringe filter (pore size 0.45 μm) to remove insoluble material to obtain the purified PNPs solution. To validate the nanoparticles for ROS responsiveness, the PNPs were incubated in phosphate-buffered saline (PBS) containing different concentrations of H_2O_2 (0, 0.1, 0.25, 0.5 and 1 mM) for 6 h. At predetermined time points, the transmittance at 500 nm was measured separately by UV spectrophotometer and the respective percentage of hydrolysis was calculated.

For preparation of PNPs@Cur, we dissolved the lyophilized carrier material with Cur in anhydrous DMSO at a ratio of 6:1 (w/w). The solution was dialyzed in pure water (MW: 8000-14000 Da) to remove the free drug and organic solvents. A portion of the resulting PNPs@Cur solution was taken and stored at 4°C, and the rest was freeze-dried for subsequent experiments. Subsequently, particle size, polydispersity index (PDI) and zeta potential were determined by dynamic light scattering (DLS) with a Delsa Nano C (Beckman Coulter, USA), morphology and size were determined by transmission electron microscopy (TEM, JEM-1400 Plus). Chitosan-based drug delivery nanosystems (CNPs@Cur) were prepared in a similar manner to the above process.

Drug encapsulation and release in vitro

The drug content in PNPs@Cur was measured by HPLC (Agilent 1260, USA)). The measurement was performed using 0.5% acetic acid aqueous solution and acetonitrile (35:65, V%) as the mobile phase with a detection wavelength of 425 nm. Then, the loading content (LC, %) and encapsulation efficiency (EE, %) are calculated according to the following equations 1 and 2, respectively.

$$LC\,(\%) = \frac{\mathrm{weightofloadeddrugs}}{\mathrm{weightofdrugloadedNPs}} \times 100\% \quad (1)$$

$$EE\,(\%) = \frac{\mathrm{weightofloadeddrug}}{\mathrm{weightofdruginfeed}} \times 100\% \quad (2)$$

The release behavior of Cur in vitro was investigated using dialysis method. For the examination of the release of PNPs@Cur in response to ROS, PNPs@Cur (5 mg) dissolved in deionized water (4 mL) were placed in dialysis bags in PBS (40 mL) containing different concentrations of H_2O_2 (0, 0.5 and 1 mM). At predetermined time points, 1 mL of the medium was taken separately for HPLC analysis and 1 mL of fresh medium was reinjected into the corresponding concentration of PBS. The cumulative release rate of Cur was calculated using the following equation 3.

$$Cumulative drug release\,(\%) = \frac{M_t}{M_0} \times 100\%\,(3)$$

where M_t is the weight of drug released at time t and M_0 is the weight of loaded Cur. The release of the experiments was performed in triplicate.

Preparation of the MM

By utilizing the Membrane Protein Extraction Kit[29, 32], we obtained purer cells membrane materials. Briefly, the collected macrophages were resuspended in membrane protein extraction buffer for 10 min under ice bath conditions, followed by transferring the cell suspension to a glass homogenizer and homogenizing about 20 times to ensure cell fragmentation. After centrifugation at 2000×g and 4°C for about 10 min, the supernatant was further centrifuged at 14000×g for about 30 min to collect the cell membrane precipitate and repeated twice to obtain purified cell membranes. Finally, the total protein content in the purified MM was analyzed by the bicinchoninic acid assay (BCA) protein assay. The prepared membrane material was stored at -80°C for future studies.

Preparation of characterization MNPs and MNPs@Cur

MNPs and MNPs@Cur were prepared by membrane extrusion[28, 29]. In brief, MM vesicles were mixed with PNPs and PNPs@Cur (1:5, w/w), followed by substantial sonication for 2 min using a bath sonicator at 40 kHz and 100 W power. Finally, nanoparticles with MM coating were obtained by repeated extrusion through 400, 200 nm polycarbonate porous membranes sequentially for at least 30 times by a micro-extruder (LiposoEasy LE-1, USA).

Then, particle size, PDI and zeta potential were also measured by DLS, as well as morphology by TEM. For further validation of the successful coating of cell membranes, the particular membrane proteins on the surface of macrophages were characterized by Western blotting. Total protein was extracted from macrophages, MM and MNPs by using a protein extraction kit, respectively, and protein concentration was determined by BCA protein assay. Approximately 25 μg of protein was subsequently added to protein loading buffer, boiled for 10 min, and then electrophoresed on a 10% sodium dodecyl sulfate polyacrylamide gel and transferred to PVDF membranes. Primary and secondary antibodies were added sequentially after closure with 5% skim milk powder, incubated for 2 h at room temperature, and specific bands were observed with an enhanced chemiluminescence detection kit.

Cytotoxicity and hemolysis assay

The cytotoxicity of PNPs and MNPs were investigated by incubation in RAW264.7 (mouse mononuclear macrophage leukemia cells) and HUVECs (human umbilical vein endothelial cells) cells. Simply, cell densities of approximately 8000 cells per well were inoculated in 96-well plates, respectively, and after overnight incubation, the medium was replaced with fresh medium containing different concentrations of PNPs or MNPs. After continued incubation for 48 h at 37°C in a cell incubator containing 5% CO_2, MTT (5 mg/mL) reagent was added and incubated for another 4 h. Then, the supernatant was removed and

DMSO was added to dissolve the bottom residue. The absorbance of each solution was read by multi-wall plate reader at 570 nm to obtain the corresponding cell viability.

As previously reported, direct contact method was used to detect the hemolytic properties of PNPs and MNPs in vitro. Briefly, 2% erythrocyte suspensions were prepared by taking blood from the orbits of mice. Then, 0.5 mL of the red cell suspension was mixed well with saline, purified water, PNPs and MNPs solutions (0.5 mL, 2 mg/mL), respectively. These specimens were then incubated continuously at 37°C for 2 hours. The absorbance of the supernatant was measured at 570 nm using a microplate reader to determine the hemoglobin released from the lysed erythrocytes. Saline and pure water were used as negative and positive controls, respectively.

In vitro binding and intracellular drug release

The targeting ability of MNPs was further investigated employing in vitro cellular uptake assays. Cellular escape ability was studied first in normal macrophages. An appropriate number of cells were seeded in 12-well plates, cultured overnight, and the original medium was replaced with fresh medium containing free Cur, PNPs@Cur, and MNPs@Cur. After incubation for 1-4 hours, respectively, the cells were washed three times with PBS, then fixed with 4% paraformaldehyde for 15 minutes, then washed three times with PBS, and finally stained with DAPI for 10 minutes and washed three times before observation by microscopy cell uptake. To imitate the inflammatory cell model[23], macrophages as well as HUVECs were activated with lipopolysaccharide (LPS,100ng/mL), respectively, and the subsequent steps were performed as described above to observe the targeting ability of MNPs@Cur in inflammatory cells. Likewise, in order to verify the potential role of PGP as priming components of Platycodon grandiflorum, the ability of PNPs@Cur and CNPs@Cur was compared respectively in terms of their uptake by macrophages in different states.

To explore further the intracellular drug release behavior, another fluorescent probe, NR, was selected to be loaded into the nanoparticles. NR did not fluoresce on its own, but excited intense fluorescence when it came into contact with intracellular lipids. The activated macrophages were obtained by LPS pretreatment, and the uptake was observed by replacing the original medium with medium containing PNPs@NR and MNPs@NR after 1, 2, 4 and 8 hours of continuous incubation.

Animals

Female BALB/c mice (6-8 weeks old, 16-18 g) were purchased from Jinan Pengyue Laboratory Animal Breeding Co. All mice were acclimatized to their environment for at least 7 days prior to the experiments. A protocol for animal use was followed by the China Animal Protection Commission and Yantai University for all animal-related procedures. All experiments on animals complied with ethical guidelines.

Animal model induction and treatment

Acute lung injury (ALI) mouse models were established according to the relevant literature. Mice were injected intraperitoneally with LPS (10 mg/kg), and after 5 h of successful modeling, randomly grouped

(n=3) and treated with intravenous saline, free Cur, PNPs@Cur and MNPs@Cur, respectively, and euthanized at 24 h after treatment for subsequent experimental analysis.

In vivo targeting to inflammatory site

After establishment of ALI mice, the mice were randomly grouped and injected intravenously with fluorescent dyes DiR (1,1-dioctadecyl-3,3,3,3-tetramethylindotricarbocyaine iodide), CNPs@DiR, PNPs@DiR and MNPs@DiR, respectively, and normal mice were used as the control group, and the fluorescence distribution of organs in each group was observed by imaging the collected organs at predetermined times with the in vivo imaging system (IVIS).

Cytokine assay

The levels of cytokines (IL-6 and TNF-α) in cell supernatants and lung tissue homogenate samples of different treatment groups were measured according to the ELISA KIT instruction manual.

Evaluation of oxidative stress in lung tissue

The lung tissues were collected from different treatment groups for weighing and then 10% lung tissue homogenates were prepared. The levels of MPO and MDA were measured according to the procedure of the relevant kit.

Lung wet/dry ratios

The lung tissues from the mice in the different treatment groups were removed and weighed immediately to obtain wet weights, followed by drying the tissue samples in an oven at 50°C to a constant weight. Finally, the degree of pulmonary edema was quantified by the ratio of wet weight to dry weight.

Histopathological analysis

For histological analysis, major organs (heart, liver, spleen, lung and kidney) were collected after different treatments, fixed overnight in 4% paraformaldehyde and paraffin embedded, then sectioned and stained with hematoxylin-eosin (H&E) for tissue evaluation.

Statistical analysis

The results obtained are expressed as mean ± SD, all statistical analyses were acquired by using GraphPad Prism version 8.0 software (GraphPad, USA). One-way ANOVA and two-way ANOVA were utilized for statistical analysis. Significance levels were set at *P < 0.05, **P < 0.01 and ***P < 0.001. Expression of all fluorescence intensities in the experiments were further calculated by Image J software.

Abbreviations

ALI:Acute lung injury

AP:Angelica polysaccharide

ARDS: Acute respiratory distress syndrome

BCA:Bicinchoninic Acid Assay

CDI: N, N'-carbonyl diimidazole

COVID-19:The novel coronavirus disease 2019

CCR2:C-C Motif Chemokine Receptor 2

CCR6:C-C Motif Chemokine Receptor 6

CXCR1:C-X-C chemokine receptor type 1

Cur:Curcumin

DAPI:4',6-diamidino-2-phenylindole

DLC:Drug loading efficiency

DLS:Dynamic light scattering

DiR:1,1-dioctadecyl-3,3,3,3-tetramethylindotricarbocyaine iodide

EE:Encapsulation efficiency

ELISA:Enzyme linked immunosorbent assay

FT-IR:Fourier transform infrared spectroscopy

FBS:Fetal bovine serum

H&E:Hematoxylin-eosin

HPLC:High Performance Liquid Chromatography

HUVECs:Human umbilical vein endothelial cells

IME:Inflammatory microenvironment

IL-6:Interleukin- 6

IVIS:Interactive Video Information System

LPS:Lipopolysaccharide

MCP-1:Monocyte chemoattractant protein-1

MM:Macrophage membranes

MPO:Myeloperoxidase

MDA:Malondialdehyde

NR:Nile Red

RAW264.7:Mouse mononuclear macrophage leukemia cells

PBS:Phosphate buffered saline TCM: Traditional Chinese Medicine

PDI:Polydispersity index

PGP:Platycodon grandiflorum polysaccharide

ROS:Reactive oxygen species

TEM:Transmission electron microscopy

TNF-α:Tumor necrosis factor-α

^{1}H NMR:Nuclear magnetic resonance hydrogen spectroscopy

4-PBAP:4-hydroxymethyl phenylboronic acid pinacol ester

ALI:Acute lung injury

AP:Angelica polysaccharide

ARDS: Acute respiratory distress syndrome

BCA:Bicinchoninic Acid Assay

CDI: N, N'-carbonyl diimidazole

COVID-19:The novel coronavirus disease 2019

CCR2:C-C Motif Chemokine Receptor 2

CCR6:C-C Motif Chemokine Receptor 6

CXCR1:C-X-C chemokine receptor type 1

Cur:Curcumin

DAPI:4',6-diamidino-2-phenylindole

DLC:Drug loading efficiency

DLS:Dynamic light scattering

DiR:1,1-dioctadecyl-3,3,3,3-tetramethylindotricarbocyaine iodide

EE:Encapsulation efficiency

ELISA:Enzyme linked immunosorbent assay

FT-IR:Fourier transform infrared spectroscopy

FBS:Fetal bovine serum

H&E:Hematoxylin-eosin

HPLC:High Performance Liquid Chromatography

HUVECs:Human umbilical vein endothelial cells

IME:Inflammatory microenvironment

IL-6:Interleukin- 6

IVIS:Interactive Video Information System

LPS:Lipopolysaccharide

MCP-1:Monocyte chemoattractant protein-1

MM:Macrophage membranes

MPO:Myeloperoxidase

MDA:Malondialdehyde

NR:Nile Red

RAW264.7:Mouse mononuclear macrophage leukemia cells

PBS:Phosphate buffered saline TCM: Traditional Chinese Medicine

PDI:Polydispersity index

PGP:Platycodon grandiflorum polysaccharide

ROS:Reactive oxygen species

TEM:Transmission electron microscopy

TNF-α:Tumor necrosis factor-α

^{1}H NMR:Nuclear magnetic resonance hydrogen spectroscopy

4-PBAP:4-hydroxymethyl phenylboronic acid pinacol ester

ALI:Acute lung injury

AP:Angelica polysaccharide

ARDS: Acute respiratory distress syndrome

BCA:Bicinchoninic Acid Assay

CDI: N, N'-carbonyl diimidazole

COVID-19:The novel coronavirus disease 2019

CCR2:C-C Motif Chemokine Receptor 2

CCR6:C-C Motif Chemokine Receptor 6

CXCR1:C-X-C chemokine receptor type 1

Cur:Curcumin

DAPI:4',6-diamidino-2-phenylindole

DLC:Drug loading efficiency

DLS:Dynamic light scattering

DiR:1,1-dioctadecyl-3,3,3,3-tetramethylindotricarbocyaine iodide

EE:Encapsulation efficiency

ELISA:Enzyme linked immunosorbent assay

FT-IR:Fourier transform infrared spectroscopy

FBS:Fetal bovine serum

H&E:Hematoxylin-eosin

HPLC:High Performance Liquid Chromatography

HUVECs:Human umbilical vein endothelial cells

IME:Inflammatory microenvironment

IL-6:Interleukin- 6

IVIS:Interactive Video Information System

LPS:Lipopolysaccharide

MCP-1:Monocyte chemoattractant protein-1

MM:Macrophage membranes

MPO:Myeloperoxidase

MDA:Malondialdehyde

NR:Nile Red

RAW264.7:Mouse mononuclear macrophage leukemia cells

PBS:Phosphate buffered saline TCM: Traditional Chinese Medicine

PDI:Polydispersity index

PGP:Platycodon grandiflorum polysaccharide

ROS:Reactive oxygen species

TEM:Transmission electron microscopy

TNF-α:Tumor necrosis factor-α

^{1}H NMR:Nuclear magnetic resonance hydrogen spectroscopy

4-PBAP:4-hydroxymethyl phenylboronic acid pinacol ester

Declarations

Availability of date and materials

All date generated or analyzed during this study are included in this published article.

Acknowledgements

All authors acknowledge financial support from Taishan Scholar Foundation of Shandong Province (No.qnts20161035), Natural Science Foundation of Shandong Province (No.ZR2019ZD24, ZR2019YQ30), Graduate Innovation Foundation of Yantai University, GIFYTU. We would also like to thank Editage (www.editage.cn) for English language editing.

Funding

This work was supported by theTaishan Scholar Foundation of Shandong Province (No. qnts20161035), Natural Science Foundation of Shandong Province (No. ZR2019ZD24, ZR2019YQ30).

Contributions

YiLi:Conceptualization, Data curation, Formal analysis, Investigation, Visualization,Writing-original draft.**Chunjing Guo**:Visualization, Writing-original draft.**Qiang Chen**:Visualization, Data curation.**YanguoSu**:Visualization, Data curation.**HuiminGuo**:Visualization, Data curation.**DaquanChen**:Conceptualization, Data curation, Funding acquisition, Methodology, Project administration, Resources, Supervision, Validation,Writing-review & editing.

Ethics approval and consent to participate

All procedures involving laboratory animals are performed in accordance with the ethics committee guidelines at the Yantai University.

Competing interests

The authors declare no competing interests.

Consent for publication

All authors agreed to publish this manuscript.

References

1. Butt Y, Kurdowska A, Allen TCJAoP, Medicine L: **Acute Lung Injury: A Clinical and Molecular Review.** 2016, **140:**345-350.
2. Tang L, Yin Z, Hu Y, Mei HJFiI: **Controlling Cytokine Storm Is Vital in COVID-19.** 2020, **11**.
3. Copaescu FA, Smibert FO, Ag B, Elizabeth J. Phillips MD F, FRACP b c, Jason A. Trubiano MBBS B, PhD, FRACP a d e f %J Journal of Allergy, Immunology C: **The role of IL-6 and other mediators in the cytokine storm associated with SARS-CoV-2 infection.** 2020, **146:**535-536.
4. Karki R, Sharma BR, Tuladhar S, Williams EP, Zalduondo L, Samir P, Zheng M, Sundaram B, Banoth B, Malireddi RJC: **Synergism of TNF-α and IFN-γ Triggers Inflammatory Cell Death, Tissue Damage, and Mortality in SARS-CoV-2 Infection and Cytokine Shock Syndromes.** 2020.

5. Hu Y, Wang T, Hu Z, Wang X, Peng PJB, Pharmacotherapy: **Clinical efficacy of glucocorticoid on the treatment of patients with COVID-19 pneumonia: A single-center experience.** 2020, **130:**110529.
6. Siemieniuk RA, Bartoszko JJ, Long G, Zeraatkar D, Brignardello-Petersen RJB: **Drug treatments for covid-19: living systematic review and network meta-analysis.** 2020, **370:**m2980.
7. Oray M, Abusamra K, Ebrahimiadib N, Meese H, Foster CSJEOoDS: **Long-term side effects of glucocorticoids.** 2016, **15:**457-465.
8. Caplan A, Fett N, Rosenbach M, Werth VP, Micheletti RGJJotAAoD: **Prevention and management of glucocorticoid-induced side effects: A comprehensive review: Infectious complications and vaccination recommendations.** 2017.
9. Ware LB, Matthay MAJNEJoM: **The acute respiratory distress syndrome.** 2012, **332:**27-37.
10. Lu Q, Yang J, Liu Z, Gutierrez C, Rouby JJJAJoR, Medicine CC: **Nebulized ceftazidime and amikacin in ventilator-associated pneumonia caused by Pseudomonas aeruginosa.** 2011, **184:**106.
11. Mata R, Yao Y, Cao W, Ding J, Gao CJR: **The Dynamic Inflammatory Tissue Microenvironment: Signality and Disease Therapy by Biomaterials.** 2021, **2021:**1-31.
12. Sfanos KS, Yegnasubramanian S, Nelson WG, Marzo ADJNRU: **The inflammatory microenvironment and microbiome in prostate cancer development.** 2018.
13. Chen J, Wang YK, Gao Y, Hu LS, Cao YBJB, Pharmacotherapy: **Protection against COVID-19 injury by Qingfei Paidu decoction via anti-viral, anti-inflammatory activity and metabolic programming.** 2020, **129:**110281.
14. Xin S, Cheng X, Zhu B, Liao X, Yu RJB, Pharmacotherapy: **Clinical Retrospective Study on the Efficacy of Qingfei Paidu Decoction Combined with Western Medicine for COVID-19 Treatment.** 2020, **129:**110500.
15. Ren JL, Zhang AH, Wang XJJPR: **Traditional Chinese medicine for COVID-19 treatment.** 2020, **155:**104743.
16. Rattis B, Ramos SG, Celes MJFiP: **Curcumin as a Potential Treatment for COVID-19.** 2021, **12:**675287.
17. Zhang Q, Wu D, Wu J, Ou Y, Mu C, Han B, Zhang QJJoE: **Improved blood–brain barrier distribution: Effect of borneol on the brain pharmacokinetics of kaempferol in rats by in vivo microdialysis sampling.** 2015, **162:**270-277.
18. Wang L, Zhao X, Du J, Liu M, Hu KJN: **Improved brain delivery of pueraria flavones via intranasal administration of borneol-modified solid lipid nanoparticles.** 2019, **14:**2105-2119.
19. Leng J, Zou L, Yi-Bing HU, Peng LX, Yu-Biao MA, Zhao GJCJoETMF: **Progress in Traditional Chinese Medicine Guide Theory and Drug Targeting.** 2011.
20. Guo C, Hou X, Liu Y, Zhang Y, Chen DJP: **Novel Chinese Angelica Polysaccharide Biomimetic Nanomedicine to Curcumin Delivery for Hepatocellular Carcinoma Treatment and Immunomodulatory Effect.** 2021, **80:**153356.

21. Sheng Y, Liu G, Wang M, Lv Z, Du PJIJoBM: **A selenium polysaccharide from Platycodon grandiflorum rescues PC12 cell death caused by H2O2 via inhibiting oxidative stress.** 2017, **104:**393-399.
22. Zhao X, Wang Y, Peng Y, Cheng G, Wang C, Geng N, Wang X, Liu JJM: **Effects of Polysaccharides from Platycodon grandiflorum on Immunity-Enhancing Activity In Vitro.** 2017, **22**.
23. Ma Q, Fan Q, Xu J, Bai J, Wang CJM: **Calming Cytokine Storm in Pneumonia by Targeted Delivery of TPCA-1 Using Platelet-Derived Extracellular Vesicles.** 2020, **3**.
24. Tang S, Zhang F, Gong H, Wei F, Wang JJSR: **Enzyme-powered Janus platelet cell robots for active and targeted drug delivery.** 2020, **5:**eaba6137.
25. Zhang W, Wang M, Tang W, Wen R, Zhou S, Lee C, Wang H, Jiang W, Delahunty IM, Zhen ZJAM: **Nanoparticle-Laden Macrophages for Tumor-Tropic Drug Delivery.** 2018, **30:**1805557.1805551-1805557.1805511.
26. Kuang S, He F, Liu G, Sun X, Zhang MJB: **CCR2-engineered mesenchymal stromal cells accelerate diabetic wound healing by restoring immunological homeostasis.** 2021**:**120963.
27. Nywening TM, Belt BA, Cullinan DR, Panni RZ, Han BJ, Sanford DE, Jacobs RC, Ye J, Patel AA, Gillanders WEJG: **Targeting both tumour-associated CXCR2+ neutrophils and CCR2+ macrophages disrupts myeloid recruitment and improves chemotherapeutic responses in pancreatic ductal adenocarcinoma.** 2018**:**gutjnl-2017-313738.
28. Gao C, Huang Q, Liu C, Kwong C, Wang RJNC: **Treatment of atherosclerosis by macrophage-biomimetic nanoparticles via targeted pharmacotherapy and sequestration of proinflammatory cytokines.** 2020, **11**.
29. Wang Y, Zhang K, Li T, Maruf A, Qin X, Luo L, Zhong Y, Qiu J, McGinty S, Pontrelli G, et al: **Macrophage membrane functionalized biomimetic nanoparticles for targeted anti-atherosclerosis applications.***Theranostics* 2021, **11:**164-180.
30. Wei X, Ran D, Campeau A, Xiao C, Zhang LJNL: **Multiantigenic Nanotoxoids for Antivirulence Vaccination against Antibiotic-Resistant Gram-Negative Bacteria.** 2019, **19**.
31. Tang M, Ping H, Qiang Z, Nanobiotechnology NTJJo: **Polymeric micelles with dual thermal and reactive oxygen species (ROS)-responsiveness for inflammatory cancer cell delivery.** 2017, **15**.
32. Cao H, Dan Z, He X, Zhang Z, Yu H, Yin Q, Li YJAN: **Liposomes Coated with Isolated Macrophage Membrane Can Target Lung Metastasis of Breast Cancer.** 2016, **10:**7738.
33. Diwanji N, Bergmann AJNC: **Basement membrane damage by ROS- and JNK-mediated Mmp2 activation drives macrophage recruitment to overgrown tissue.** 2020, **11**.
34. Nie Y, Wang Z, Chai G, Xiong Y, Zhao PJM: **Dehydrocostus Lactone Suppresses LPS-induced Acute Lung Injury and Macrophage Activation through NF-κB Signaling Pathway Mediated by p38 MAPK and Akt.** 2019, **24:**1510.
35. Orecchioni M, Ghosheh Y, Pramod AB, Ley KJo: **Macrophage Polarization: Different Gene Signatures in M1(LPS+) vs. Classically and M2(LPS–) vs. Alternatively Activated Macrophages.** 2019, **10**.

36. Debra L, Laskin, Rama, Malaviya, Toxicology DJJTsaojotSo: **Role of Macrophages in Acute Lung Injury and Chronic Fibrosis Induced by Pulmonary Toxicants.** 2018.

37. Fan E, Brodie D, Slutsky ASJJ: **Acute Respiratory Distress Syndrome: Advances in Diagnosis and Treatment.** 2018, **319:**698-710.

38. Guo J, Li D, Tao H, Li G, Liu R, Dou Y, Jin T, Li L, Huang J, Hu H, Zhang J: **Cyclodextrin-Derived Intrinsically Bioactive Nanoparticles for Treatment of Acute and Chronic Inflammatory Diseases.** *Adv Mater* 2019, **31:**e1904607.

Figures

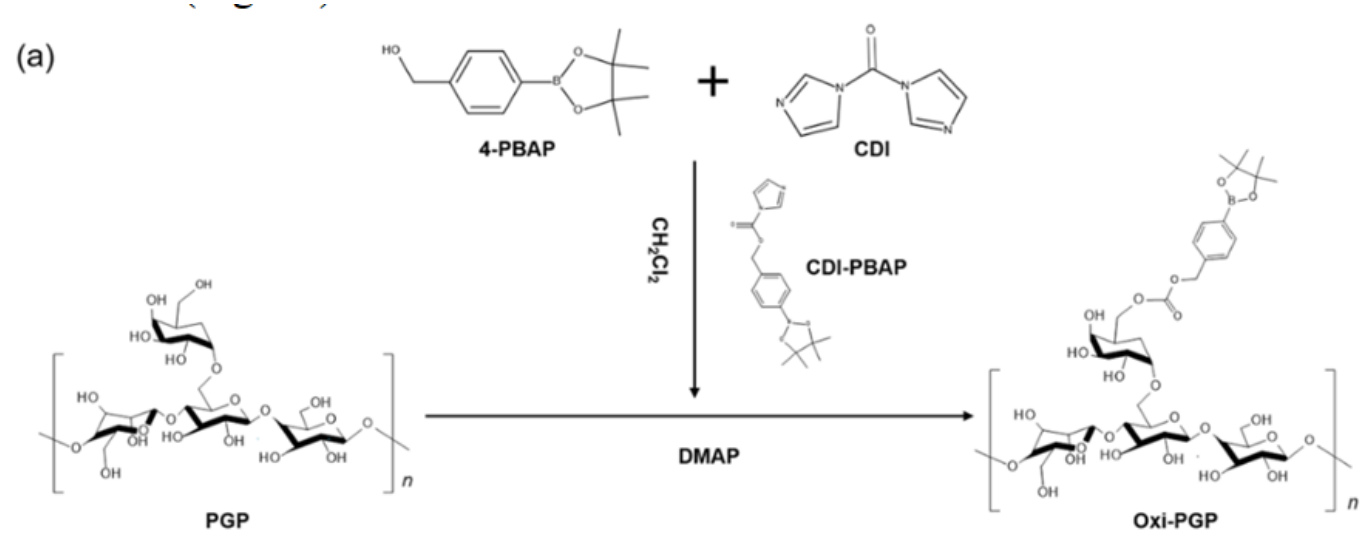

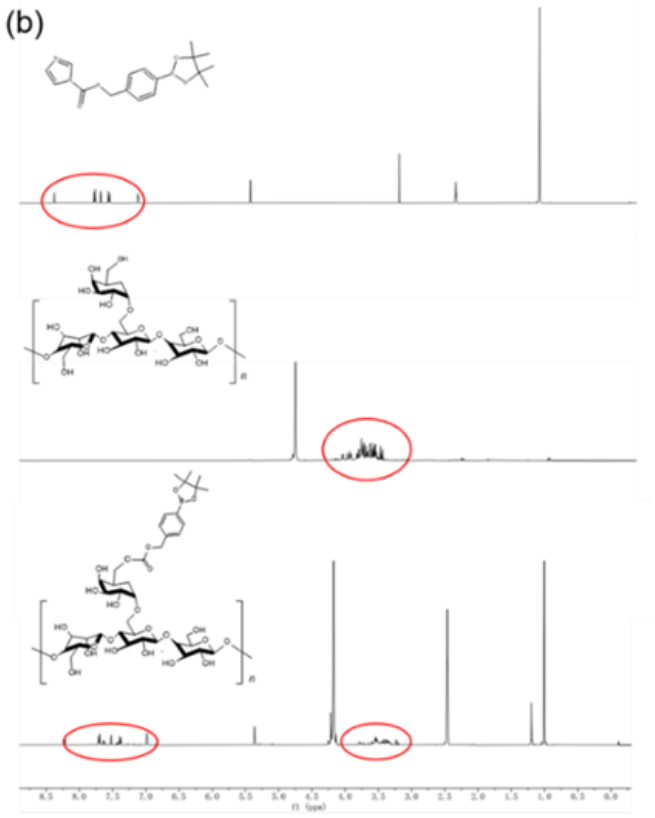

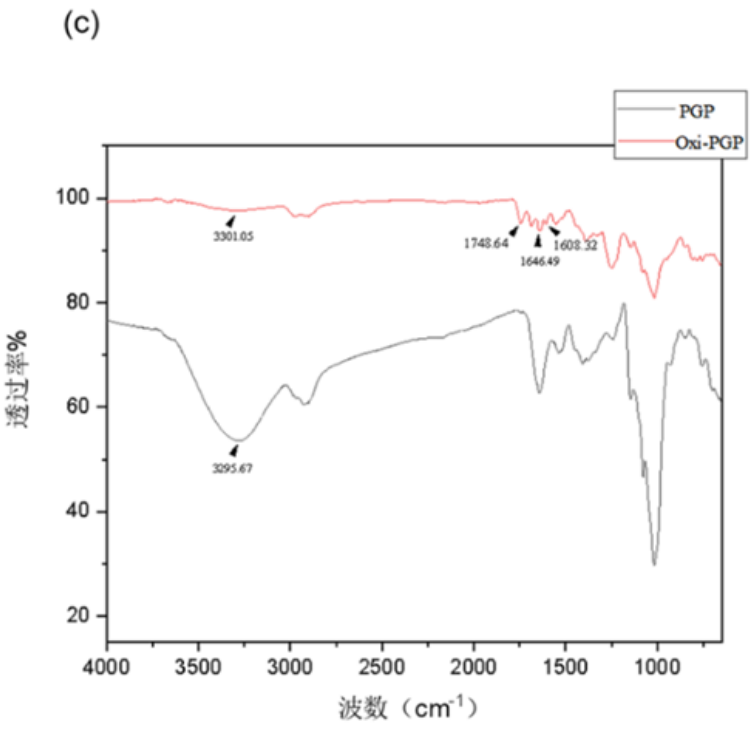

Figure 1

Synthesis and characterization of Oxi-PGP. (a) The synthesis route of Oxi-PGP. (b) 1H NMR spectrum of CDI-PBAP, PGP and Oxi-PGP. (c) FT-IR spectrum of PGP and Oxi-PGP.

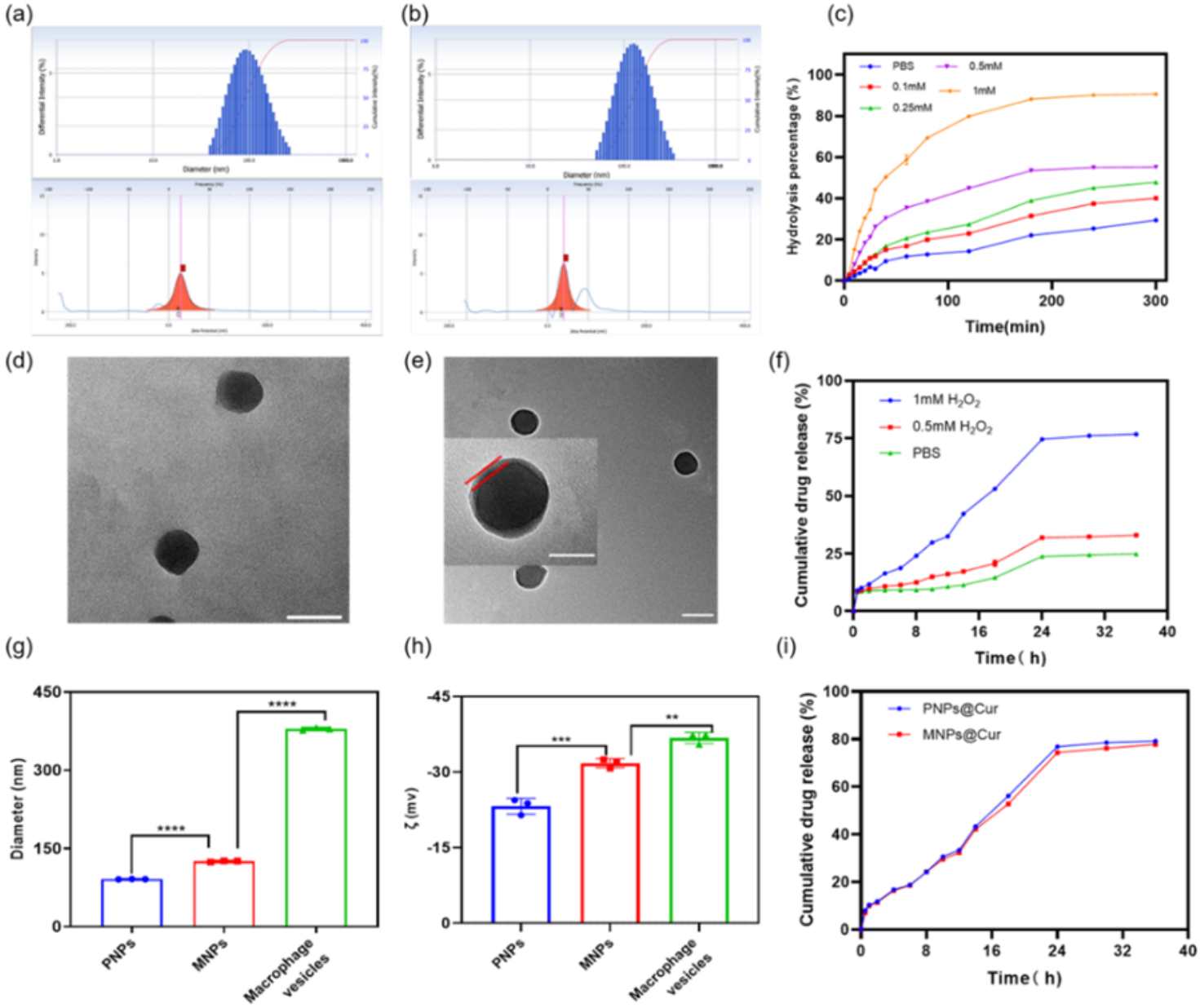

Figure 2

Preparation and characterization of ROS responsive PNPs and MNPs. (a, b) The particle size and potential of the PNPs and MNPs respective DLS. (c) Hydrolysis rates of PNPs in PBS with different concentrations of H2O2 (0, 0. 1 mM, 0.25 mM, 0.50 mM and 1.00 mM). (d) TEM images of representative PNPs. Scale bar. 100 nm. (e) TEM images of representative MNPs. Scale bar. 100 nm. Inset: the amplified TEM image of a single MNP. Scale bar: 100 nm. (f) In vitro release of Cur from PNPs in PBS at different concentrations of H2O2 (0, 0. 5 mM and 1Mm). (g, h) Particle sizes and Zeta potentials of PNPs and MNPs analyzed by DLS. (i) In vitro drug release profiles of PNPs@Cur and MNPs@Cur. Statistical

significance was calculated by one-way ANOVA (n=3). P-value: *P < 0.05, **P < 0.01 and ***P < 0.001. Data are means ± SD.

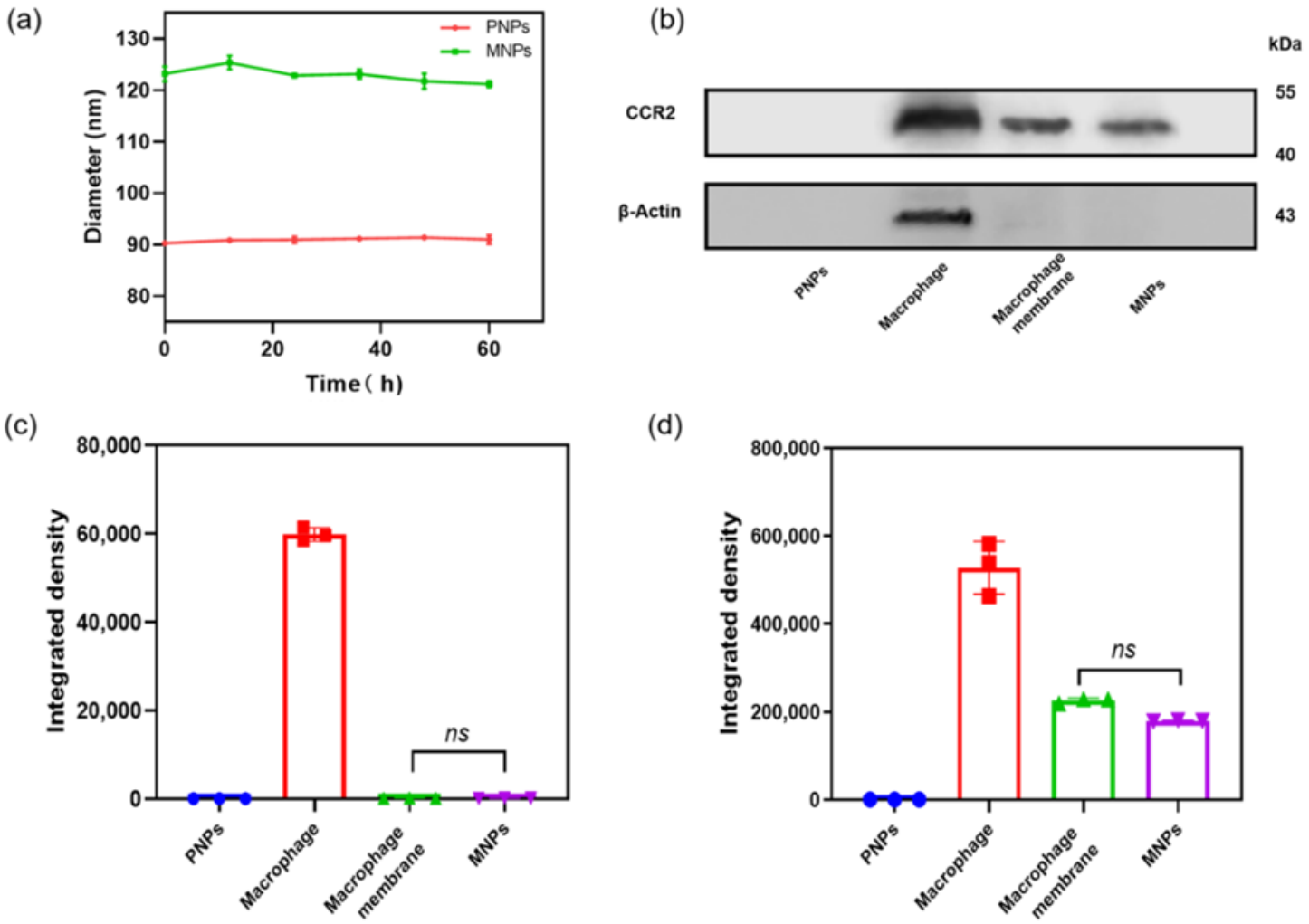

Figure 3

Stability and protein analysis. (a) The particle stability of PNPs and MNPs incubated in the buffers for 60 h at 4°C. (b-d) The protein bands characteristic of PNPs, macrophages, MM derived vesicles and MNPs were verified by Western blotting. Statistical significance was calculated by one-way ANOVA (n=3). P-value: *P < 0.05, **P < 0.01 and ***P < 0.001. Data are means ± SD.

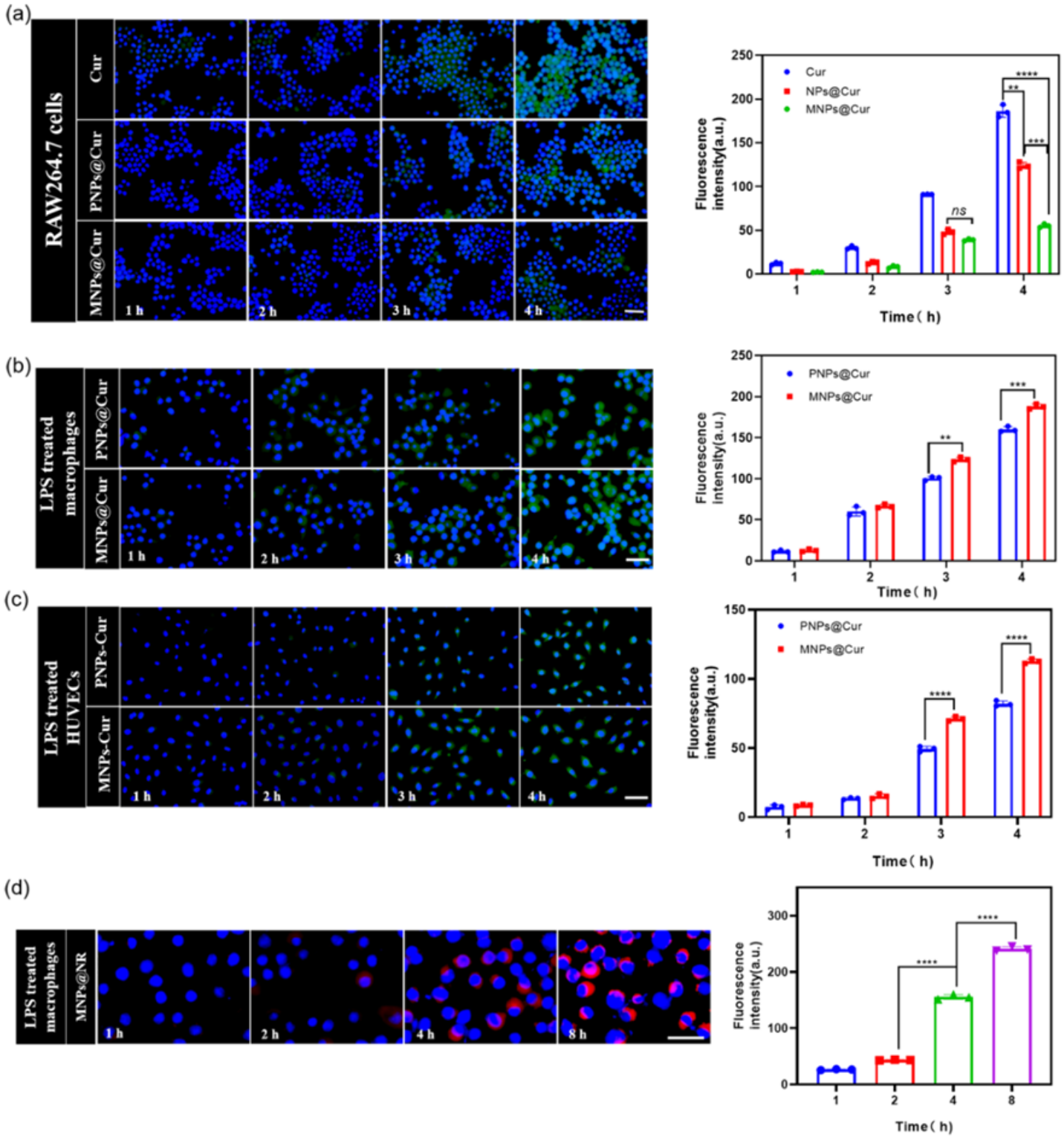

Figure 4

Capacity to target at the cellular level in vitro. (a) Ability to escape from RAW264.7 cells (including quantitative analysis) of free Cur, PNPs@Cur and MNPs@Cur. Scale bar: 50 μm. (b, c) Cellular uptake (including quantitative analysis) of PNPs@Cur and MNPs@Cur by RAW264.7 cells and HUVECs treated with LPS respectively. Scale bar: 50 μm. (d) Validated intracellular release of MNPs@NR in LPS-treated macrophages (including quantitative analysis). Scale bar: 50 μm. Statistical significance was calculated

by one-way ANOVA and two-way ANOVA (n=3-5). P value: *P < 0.05, **P < 0.01 and ***P < 0.001. Data are means ± SD.

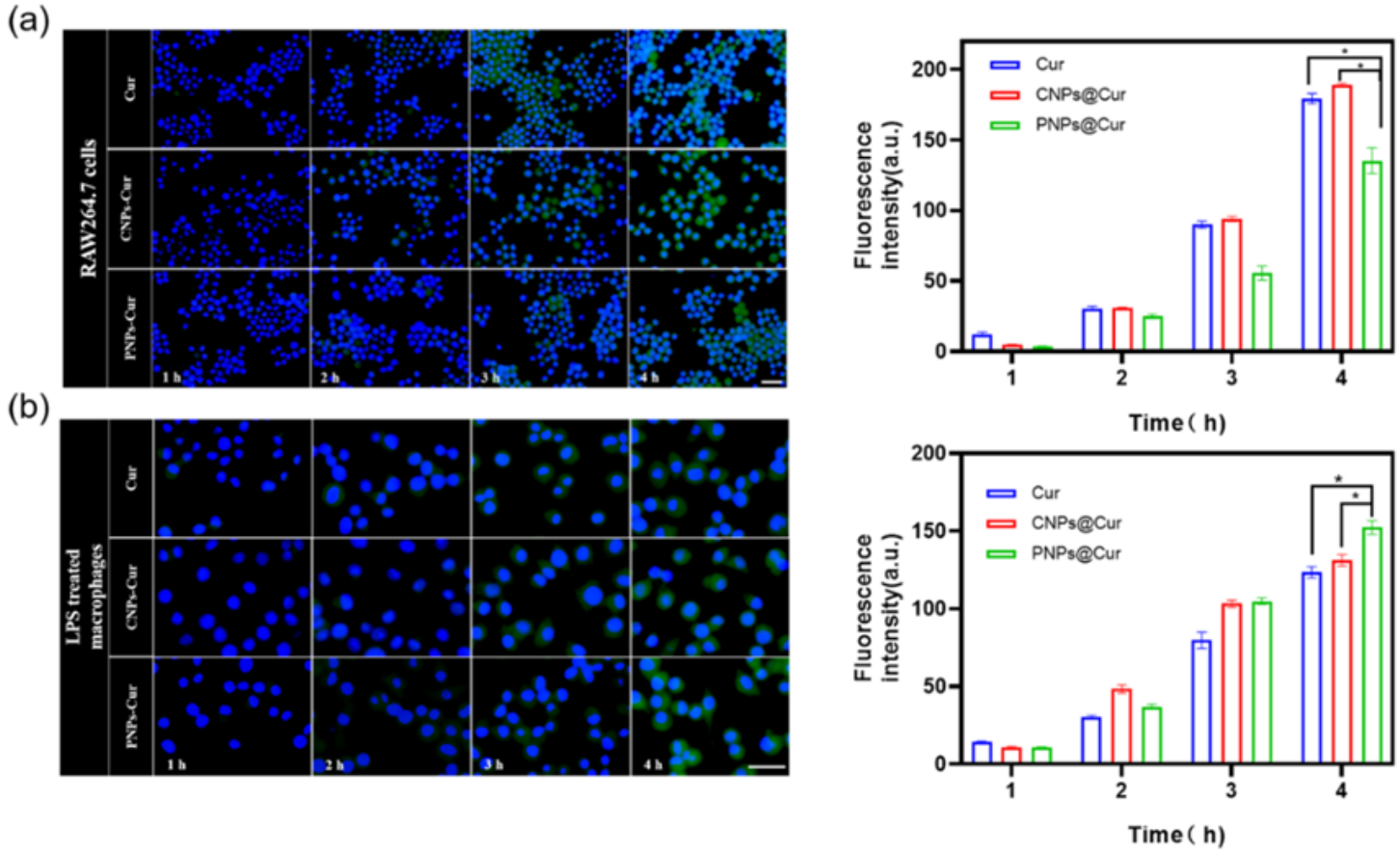

Figure 5

In vitro targeting of PNPs. (a) Ability to escape from RAW264.7 cells (including quantitative analysis) of free Cur, CNPs@Cur and PNPs@Cur. Scale bar: 50 μm. (b) Cellular uptake (including quantitative analysis) of free Cur, CNPs@Cur and PNPs@Cur by RAW264.7 cells treated with LPS. Scale bar: 50 μm. P-value: *P < 0.05. Data are means ± SD.

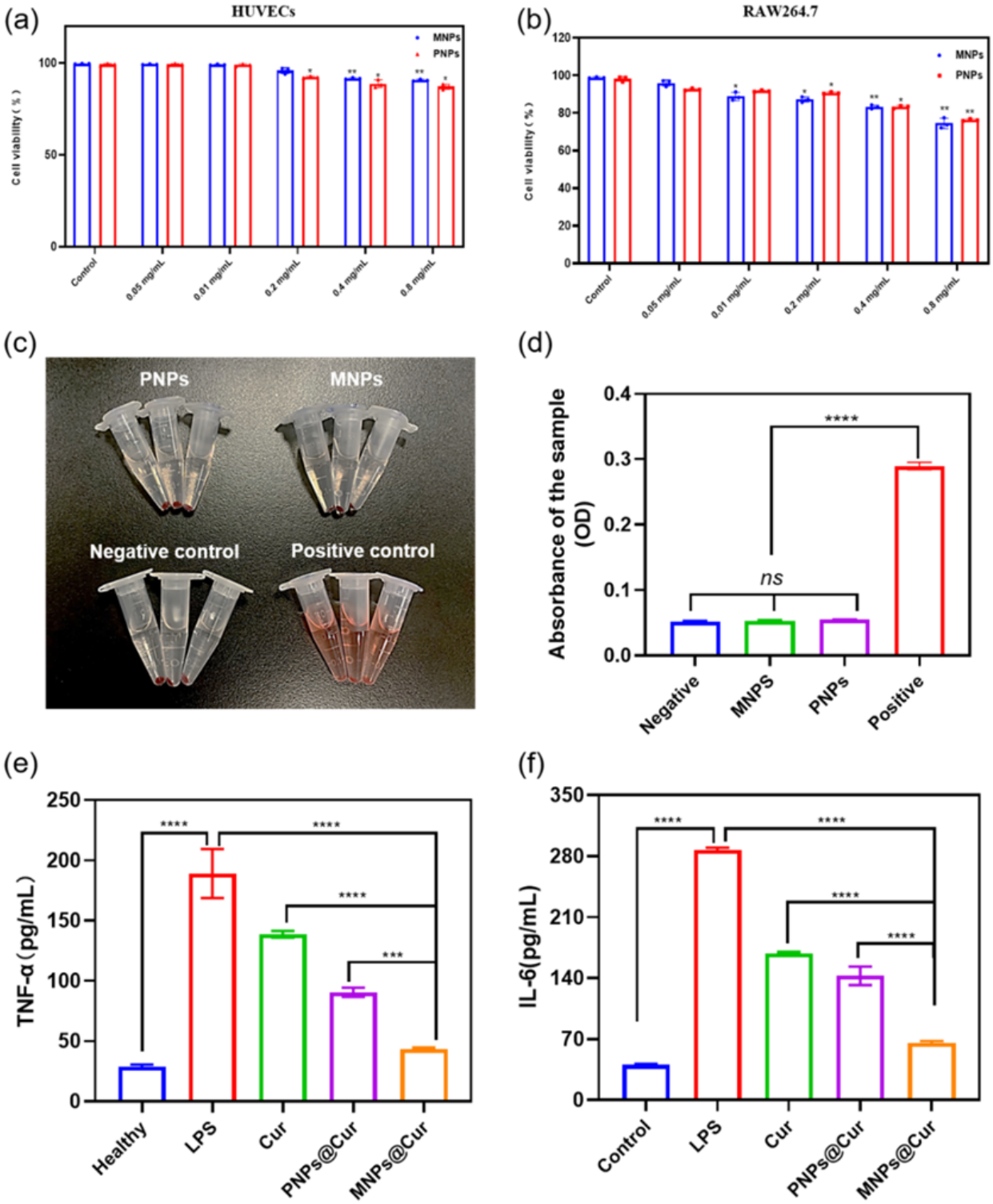

Figure 6

In vitro safety compatibility and suppression cytokine studies. (a, b) Cell viability of HUVECs andRAW264.7 cells after incubation with various doses of PNPs and MNPs for 48 h. (c) Images of the hemolysis test with PNPs and MNPs. (d) The absorbance of PNPs and MNPs measured at 570 nm. (e, f) Generation of TNF-α and IL-6 from activated macrophages supernatant after incubated with combinations of LPS (100 ng/mL), free Cur, PNPs@Cur and MNPs@Cur. Statistical significance was

calculated by two-way ANOVA and one-way ANOVA (n=3). P-value: *P < 0.05, **P < 0.01 and ***P < 0.001. Data are means ± SD.

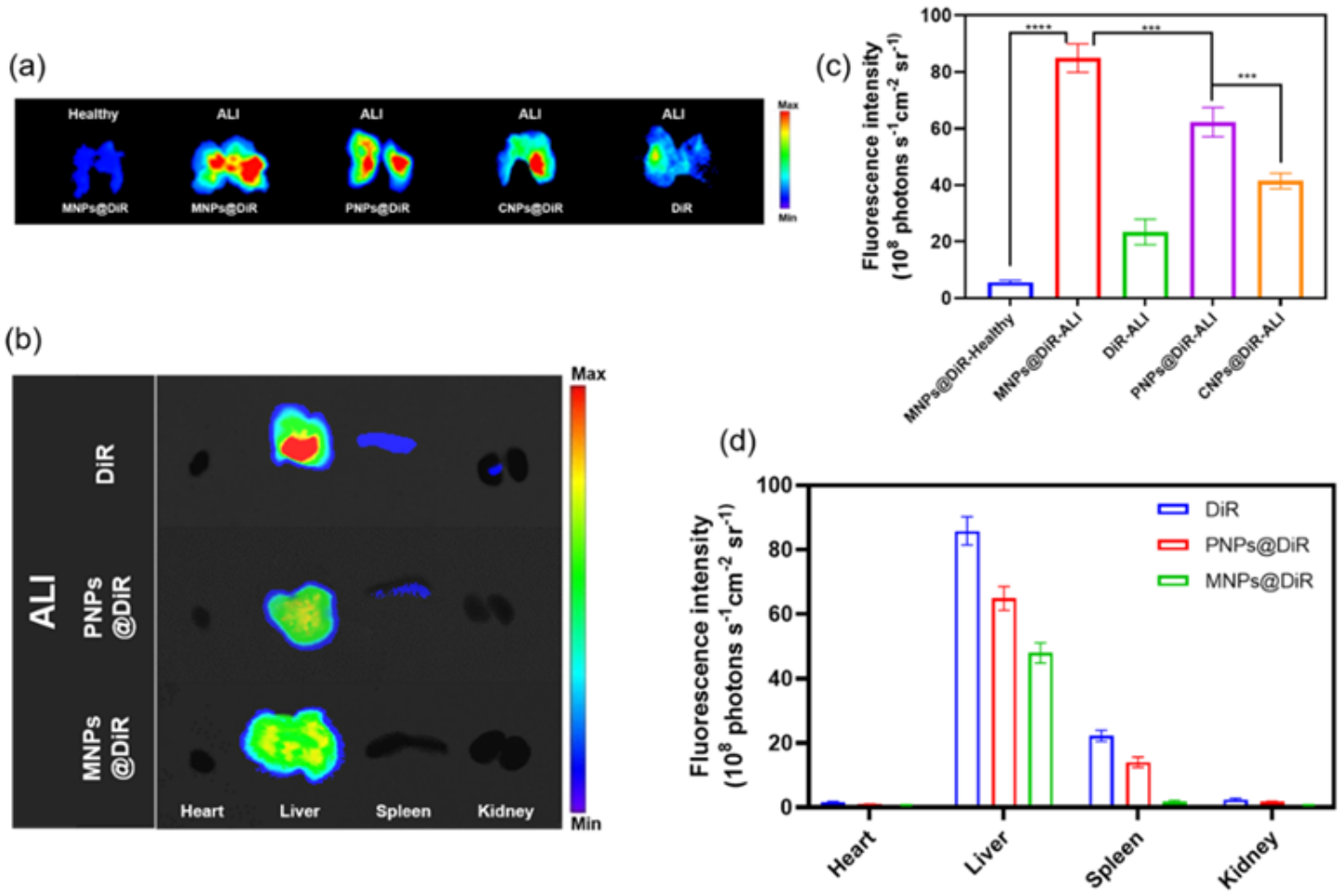

Figure 7

Targeting of impaired lungs in mice. (a, b) The biodistribution fluorescence of MNPs@DiR, MNPs@DiR and MNPs@DiR were measured using IVIS. (c, d) Quantitative analysis in lungs and other organs confirmed by IVIS. Statistical significance was calculated by two-way ANOVA and one-way ANOVA (n=3-5). P-value: *P < 0.05, **P < 0.01 and ***P < 0.001. Data are means ± SD.

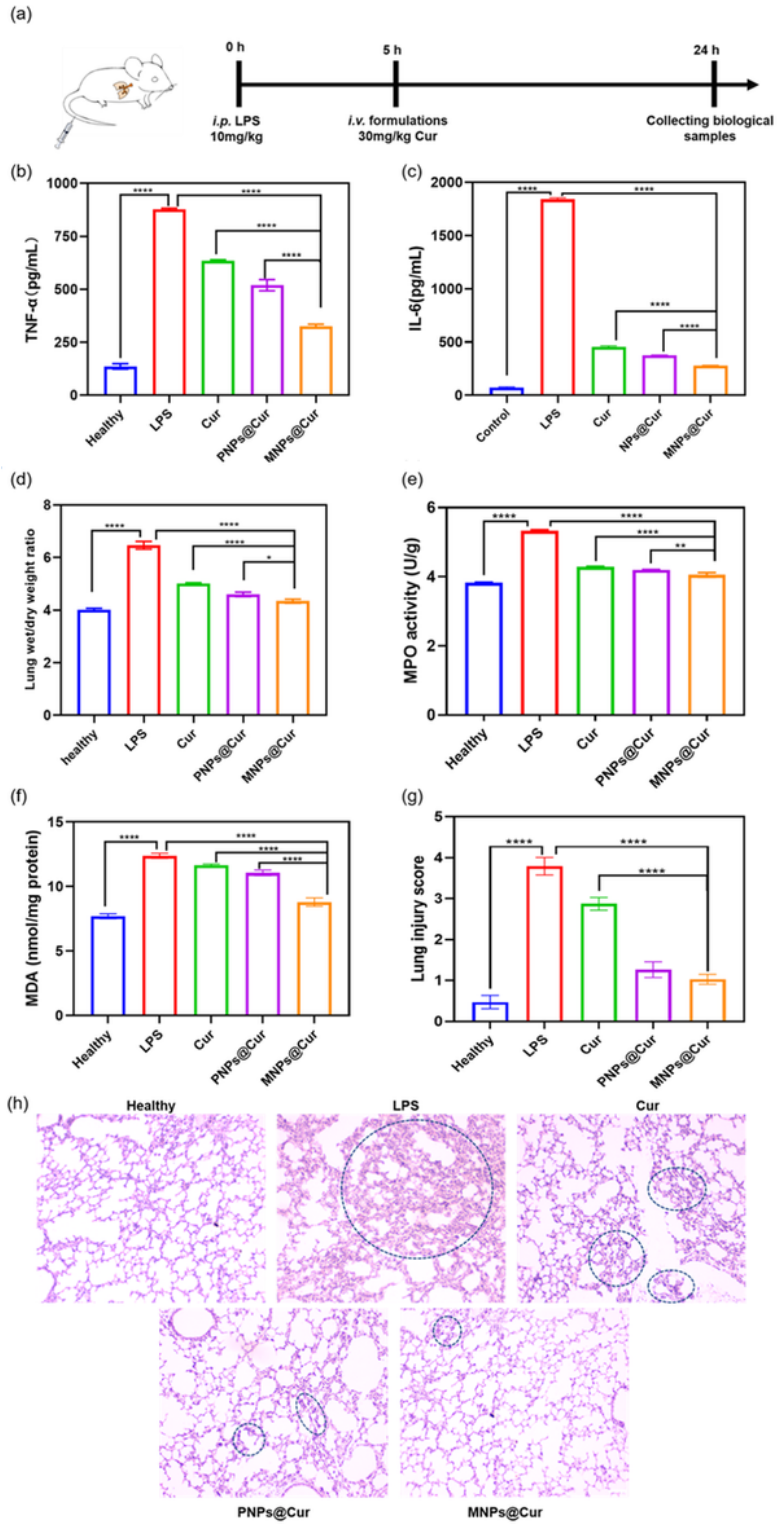

Figure 8

Targeted delivery of MNPs@Cur inhibits cytokine storm to improve lung inflammation. (a) The schedule of experiments for ALI model studies. ALI mouse models were induced by intraperitoneal injection of LPS (10 mg/kg). 5 hours after LPS administration, mice were injected intravenously with saline, free Cur, PNPs@Cur, and MNPs@Cur and 19 hours after drug administration, lungs were collected for treatment analysis. (b, c) The expression levels of inflammatory factors TNF-α, IL-6 in the lung tissue homogenate

of mice after various treatments. (d) The wet-to-dry ratios of the lungs by different treatments indicated in the diagram. (e, f) The levels of MPO and MDA in lung tissue homogenates after various treatments, as shown. (g, h) Semi-quantitative analysis of lung damage scores and H&E-stained lung tissue sections were imaged. The blue circles indicate neutrophil infiltration. Scale bar: 100 μm. Statistical significance was calculated by one-way ANOVA (n=3-5). P-value: *P < 0.05, **P < 0.01 and ***P < 0.001. Data are means ± SD.

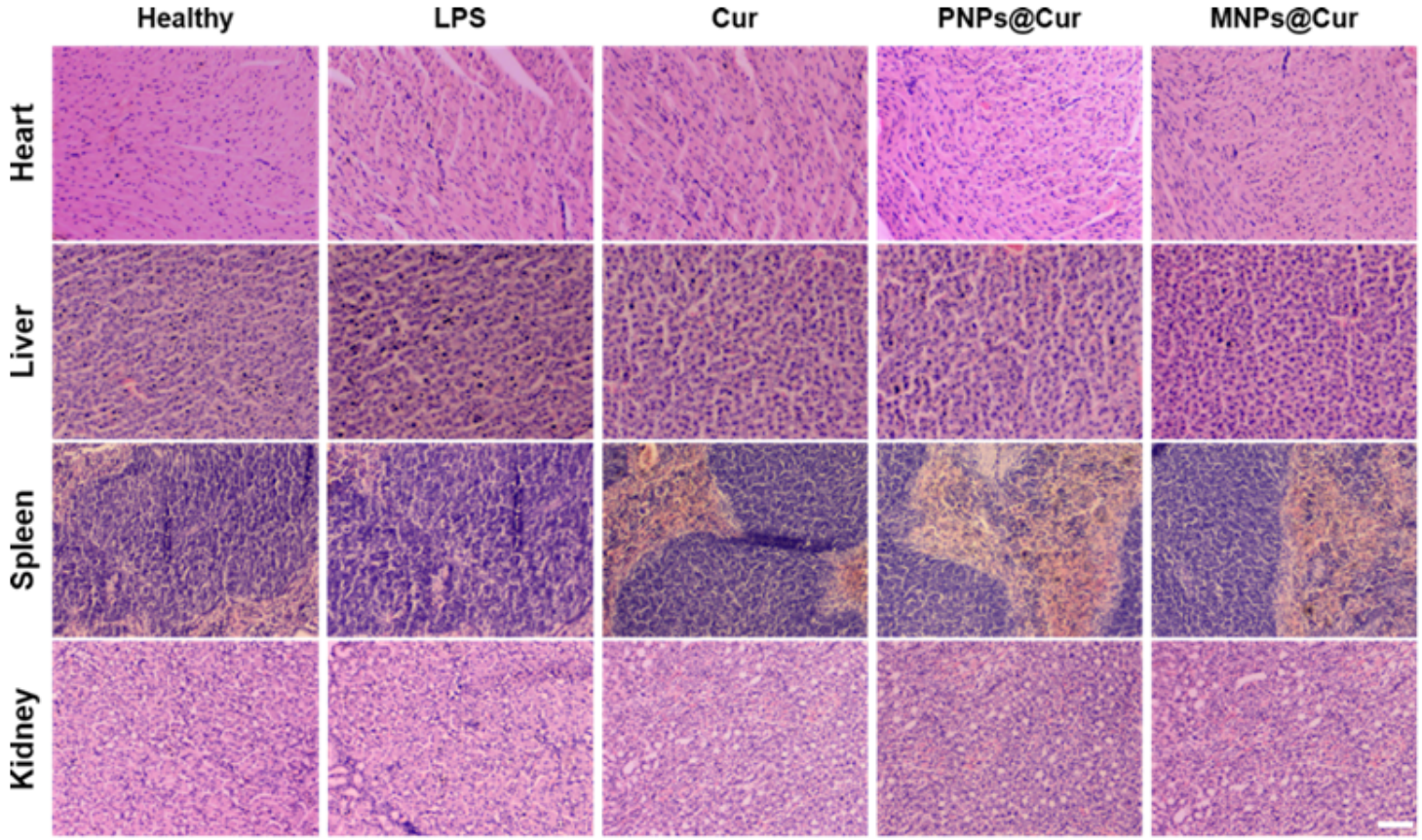

Figure 9

Samples were collected from the heart, liver, kidney and spleen, sectioned and stained (H&E) for histological analysis (scale bar = 100 μm). There were no signs of tissue damage or disorganization of tissue structure found in any of the tissues.

Supplementary Files

This is a list of supplementary files associated with this preprint. Click to download.

- Graphicalabstract1.docx
- Scheme1.png